CHEMISTRY OF MATERIALS
Article

Chem. Mater. **2010,** *22,* 2125–2131 2125
DOI:10.1021/cm903709m

Nonaqueous Route toward a Nanostructured Hybrid Titanate

David Portehault,*,† Cristina Giordano,† Clément Sanchez,‡ and Markus Antonietti†

†*Max-Planck-Institute of Colloids and Interfaces, Department of Colloid Chemistry, Research Campus Golm, 14424 Potsdam, Germany, and* ‡*UPMC Univ Paris 06, CNRS, UMR 7574, Chimie de la Matière Condensée de Paris, Collège de France, 11 place Marcelin Berthelot, 75231 Paris Cedex 05, France*

Received December 10, 2009. Revised Manuscript Received January 29, 2010

The first nonaqueous sol−gel route toward novel functional hybrid lamellar titanates is reported, enabling structural and morphological control of the nanostructured materials. The synthesis occurs at 220 °C in triethyleneglycoldimethylether (triglyme), with $TiCl_4$ and an amine−BH_3 complex (amine = ^{t}BuH$_2$N, pyridine, Me$_2$HN, Me$_3$N) as precursors. Results from elemental and energy dispersive X-ray analyses, X-ray and electron diffractions, and Raman spectroscopy suggest a distorted pseudolepidocrocite-type structure for the hybrid titanate $(N(CH_3)_4)_{0.8}Ti_2O_4(OH)_{0.8(1-x)}O_{0.4\cdot x}$ ($0 \le x \le 1$), which intercalates tetramethylammonium cations. Structural control is performed with different amine complexes, yielding selectively anatase nanoparticles or titanate nanosheets. Addition of long chain amines leads to tunable titanate morphology and surface area, ranging from 90 to 220 $m^2 \cdot g^{-1}$. Analysis of the organic byproducts enables one to elucidate the reaction pathways toward titanium-oxo species, as well as in situ formation of the interlamellar ammonium species. The hybrid titanate undergoes structural evolution upon UV exposition, together with an increase of the photocatalytic activity, thus underlining the potential of nonaqueous sol−gel chemistry for investigating structural diversity of functional titanates.

Introduction

The various modifications of titanium oxide are a centerpiece of nanomaterial science, because of significant technological applications, including photovoltaics, electrochromics, photochromics, electroluminescence, catalytic devices, and sensors. Among these compounds, alkali and protonated layered titanates with a formula $A_2Ti_nO_{2n+1}$ (A^+ = alkali metal ion or proton, $n \le 5$) and their relatives are more sparsely covered and are mostly used as precursors for efficient anatase based photocatalysts.[1,2] They also have been proven to exhibit photocatalytic activity[1,2] and hydrogen uptake capacities, as well as good cycling stability as electrode materials in Li batteries.[3] The few reported examples of hybrid titanates incorporating organic cations (ammonium NH_4^+,[4] tetramethylammonium,[5] tetrabutylammonium,[1] and polydiallyldimethylammonium[6]) highlight the potential existence of a wide range of hybrids in the titanate family. However, investigations in this area are still in their infancy because of the limited number of applicable synthetic strategies. In particular, all the reported titanates have been synthesized in water.[1,4−6] While providing an easy way to handle the reactants in an environmentally friendly solvent, aqueous synthesis of nanomaterials generally requires complex procedures because of the dual oxidant−reductant and acide−base behavior of water.[7] Most importantly, use of water as solvent considerably decreases the range of available precursors that can be used to tune the reaction pathways of solid formation. Nonaqueous methods open new challenges, enable the use of a larger set of reactants, and were recently used to drive crystallization of complex shapes and architectures.[8,9] Anatase[10] and other TiO_2 polymorphs have been synthesized with nonaqueous procedures[11−16] while, to our knowledge, no lamellar titanate synthesis was reported in an organic medium.

*To whom correspondence should be addressed. E-mail: David.Portehault@mpikg.mpg.de.

(1) Sasaki, T.; Nakano, S.; Yamauchi, S.; Watanabe, M. *Chem. Mater.* **1997**, *9*, 602–608.
(2) Peng, C.-W.; Ke, T.-Y.; Brohan, L.; Richard-Plouet, M.; Huang, J.-C.; Puzenat, E.; Chiu, H.-T.; Lee, C.-Y. *Chem. Mater.* **2008**, *20*, 2426–2428.
(3) Bavykin, D. V.; Friedrich, J. M.; Walsh, F. C. *Adv. Mater.* **2006**, *18*, 2807–2824.
(4) Takezawa, Y.; Imai, H. *Small* **2006**, *2*, 390–393.
(5) Liu, C.-E.; Rouet, A.; Sutrisno, H.; Puzenat, E.; Terrisse, H. l. n.; Brohan, L.; Richard-Plouet, M. *Chem. Mater.* **2008**, *20*, 4739–4748.
(6) Sasaki, T.; Ebina, Y.; Tanaka, T.; Harada, M.; Watanabe, M.; Decher, G. *Chem. Mater.* **2001**, *13*, 4661–4667.
(7) Portehault, D.; Cassaignon, S.; Baudrin, E.; Jolivet, J.-P. *J. Mater. Chem.* **2009**, *19*, 2407–2416.
(8) Niederberger, M.; Pinna, N. *Metal Oxide Nanoparticles in Organic Solvents: Synthesis, Formation, Assembly and Application*; Springer: London, 2009.
(9) Garnweitner, G.; Niederberger, M. *J. Mater. Chem.* **2008**, *18*, 1171–1182.
(10) Trentler, T. J.; Denler, T. E.; Bertone, J. F.; Agrawal, A.; Colvin, V. L. *J. Am. Chem. Soc.* **1999**, *121*, 1613–1614.
(11) Niederberger, M.; Bartl, M. H.; Stucky, G. D. *Chem. Mater.* **2002**, *14*, 4364–4370.
(12) Wang, C.; Deng, Z.-X.; Li, Y. *Inorg. Chem.* **2001**, *40*, 5210–5214.
(13) Polleux, J.; Pinna, N.; Antonietti, M.; Niederberger, M. *Adv. Mater.* **2004**, *16*, 436–439.
(14) Garnweitner, G.; Antonietti, M.; Niederberger, M. *Chem. Commun.* **2005**, 397–399.
(15) Garnweitner, G.; Tsedev, N.; Dierke, H.; Niederberger, M. *Eur. J. Inorg. Chem.* **2008**, *2008*, 890–895.
(16) Wu, B.; Guo, C.; Zheng, N.; Xie, Z.; Stucky, G. D. *J. Am. Chem. Soc.* **2008**, *130*, 17563–17567.

Published on Web 02/12/2010

This contribution reports the nonaqueous synthesis of a novel lamellar hybrid titanate with intercalated alkylammonium cations. The process is carried out in a polyether solvent at 220 °C, without any protic species. The reaction pathway toward these structures is investigated, thus highlighting new mechanisms for oxide formation in organic media. Use of different amine precursors leads to selective formation of anatase nanoparticles or titanate nanosheets with a pseudolepidocrocite-type structure. Textural control is shown through addition of long chain amines which provide tunable surface area of titanate materials, with the coupled modified photocatalytic activity. This work demonstrates the high potential of nonaqueous processes to explore structural and morphological diversity of titanates with specific properties.

Experimental Section

Synthesis. All synthesis and washing steps were carried out in inert atmosphere using argon saturated liquids in an argon filled glovebox and with classical Schlenk techniques. Typically, 8 mmol of an amine−BH_3 complex ($^tBuH_2N-BH_3$, pyridine−BH_3, Me_2HN-BH_3, Me_3N-BH_3, Alfa Aesar) were dissolved in 10 mL of triethyleneglycoldimethylether (triglyme, Alfa Aesar). Two millimoles of $TiCl_4$ was then added to the solution. The resulting limpid yellow solution was transferred in a stainless steel autoclave and heated to 220 °C during 17 h. To investigate the effect of long chain amines, some syntheses were performed with BH_3-NMe_3 and addition of 8 mmol of NEt_3, NPr_3, or NOc_3. The powders were then washed twice with triglyme and three times with dried EtOH and dried under vacuum during 1 day.

Techniques. *X-ray Diffraction* (*XRD*). XRD measurements were performed on a D8 Bruker apparatus operating at the Cu Kα1 radiation. Profile matching was performed using the FullProf Suite.[17,18] The anatase pattern was indexed according to the ICDD file 04-007-0701.

Fourier Transform Infrared (*FT-IR*). Infrared spectra were recording on KBr pellets using a Varian 1000 FT-IR apparatus.

Elemental analysis (*EA*). Carbon, hydrogen, and nitrogen contents were measured using a Vario EL Elementar instrument. B and Ti content were determined using ICP-OES at the Fraunhofer Institute für Angewandte Polymerforschung, Golm.

Field Emission Scanning Electron Microscopy (*FESEM*). Observations were performed on a LEO 1550-Gemini instrument. The samples were loaded on carbon coated stubs and coated by sputtering a Au/Pd alloy prior to imaging.

Transmission Electron Microscopy (*TEM*). Studies were carried out using a JEOL 100CX (100 kV) apparatus at the University Pierre et Marie Curie, Paris. Samples were prepared by evaporating a drop of diluted suspension in ethanol on a carbon-coated copper grid.

N_2 sorption. Samples were degassed at 120 °C for 20 h before measuring on a Quadrasorb apparatus at 78 K.

Photocatalysis. The photocatalytic activities were evaluated by the decomposition of 4-chlorophenol (4-CP) in an aqueous phase. The catalyst (40 mg) was suspended in 100 mL of a solution containing 40 ppm of 4-CP. A 100 W xenon lamp was used as the light source for irradiation and a glass beaker was used as the container, which cuts short wavelengths. In the range of the transmitted irradiation wavelengths ($\lambda \geq 300$ nm), 4-CP does not absorb light (see Supporting Information). The suspension was stirred in the dark for 1 h to achieve adsorption equilibrium. Then, the sample was irradiated to induce photocatalytic reactions. At given irradiation time intervals, 2 mL of the suspension was collected and then filtered to remove the catalyst. The degradated solutions were analyzed using a UV−vis spectrophotometer. The photocatalytic performance of commercial TiO_2 (Degussa P25) was also tested under the same experimental conditions as a reference. The percentage of degradation is calculated as $C(t)/C_0$, where $C(t)$ is the absorption at the maximum peak (220 nm) of the 4-CP spectra for each irradiation time interval and C_0 is the absorption of the starting solution when adsorption equilibrium is achieved.

Results and Discussion

The synthesis was carried out in triethyleneglycoldimethylether (triglyme) $CH_3(OCH_2CH_2)_3OCH_3$, at 220 °C, under inert atmosphere and autogenic pressure in an autoclave for 17 h. $TiCl_4$ as the titanium source and an amine−BH_3 complex (*tert*-butylamine−BH_3 ($^tBuH_2N-BH_3$), pyridine−BH_3, Me_2HN-BH_3, or Me_3N-BH_3) as an "activator" (molar ratio 1:4) were dissolved in triglyme prior to the heat treatment. To investigate the role of the amine alkyl chains, some syntheses were also performed in the presence of triethylamine (NEt_3), tripropylamine (NPr_3), or trioctylamine (NOc_3).

Powder XRD patterns (Figure 1a) of the products exhibit characteristic peaks of anatase with $^tBuH_2N-BH_3$ and pyridine−BH_3 as precursors. When Me_2HN-BH_3 and Me_3N-BH_3 are used, additional peaks at 7.6° (1.16 nm) and 15.3° (0.56 nm) are observed, together with a shift of a broad peak from 48.0° to 48.4°. When triethylamine NEt_3 with Me_3N-BH_3 (Figure 1b) as an intercalating agent was used, the peak at 1.16 nm with Me_3N-BH_3 as a single reactant is broadened and shifted to 1.64 nm. This reflection is then due to a mesostructure which incorporates the amine species. In the presence of tripropylamine (NPr_3) and trioctylamine (NOc_3) (Figure 1b,c), no shift is observed at 7.6° but the wide angle peaks are more resolved and indicate a more ordered structure with XRD patterns which strongly differ from anatase. In fact, these patterns are closely related to previously reported lamellar titanates.[2] The peak at 1.16 nm and its second harmonic at 0.56 nm account for the lamellar ordering of the compound with a high interlamellar distance.[19−21] However, the present patterns cannot be indexed according to previously described structures and suggest the formation of a new lamellar titanate.

In the presence of Me_2HN-BH_3 or Me_3N-BH_3 and the absence of any trialkylamines (Figure 1a), a broad

(17) Rodriguez-Carvajal, J. *Phys. B* **1993**, *192*, 55–69.
(18) http://www.ill.eu/sites/fullprof/
(19) Ma, R.; Bando, Y.; Sasaki, T. *Chem. Phys. Lett*. **2003**, *380*, 577–582.
(20) Ma, R.; Fukuda, K.; Sasaki, T.; Osada, M.; Bando, Y. *J. Phys. Chem. B* **2005**, *109*, 6210–6214.
(21) Peng, C.-W.; Richard-Plouet, M.; Ke, T.-Y.; Lee, C.-Y.; Chiu, H.-T.; Marhic, C.; Puzenat, E.; Lemoigno, F.; Brohan, L. *Chem. Mater*. **2008**, *20*, 7228–7236.

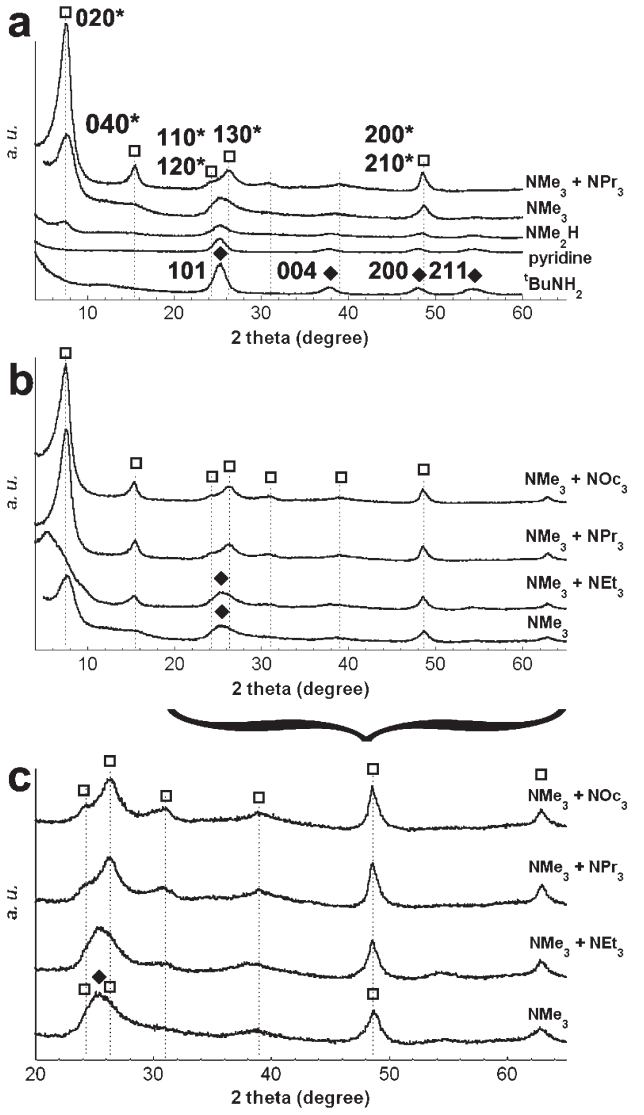

Figure 1. XRD patterns of samples obtained for (a) different amine–BH_3 precursors or (b) addition of different long chain trialkylamines to the Me_3N–BH_3 precursor. (c) Enlargement of (b). Black diamonds: anatase and corresponding indexes; empty squares: lamellar titanate and corresponding indexes obtained by cell refinement (*).

peak is observed at 25.4° which could originate from anatase TiO_2 as side products. When adding NPr_3 or NOc_3, energy dispersive X-ray (EDX) analysis performed during TEM measurements indicates that no noticeable amount of chloride is present. Elemental analysis shows a negligible boron content (B/Ti < 0.02) and a N/Ti ratio of about 0.4, confirming that the amine species are part of the structure. Elemental analysis provides a titanate formula of $A_{0.8}Ti_2O_4(OH)_{0.8(1-x)}O_{0.4\cdot x}$ ($0 \le x \le 1$), as derived from N and Ti contents, where A^+ is the interlamellar cation containing one nitrogen and various alkyl chains. As the same XRD pattern is observed for NPr_3 and NOc_3, it is assumed that the same interlamellar species are present, presumably originating from the Me_3N–BH_3 activator which is the common reactant between all the syntheses. Propyl and octyl chains of NPr_3 and NOc_3 are obviously too bulky to be incorporated between the Ti–O layers. The broad interlamellar reflection for NEt_3 and the absence of shift of the second harmonic at 0.56 nm can originate from a more statistical incorporation of cations in this case. Infrared spectra were recorded in order to further characterize the interlamellar species within the hybrid titanate (Figure SI-1 in the Supporting Information). In addition to a broadband at ca. 3200 cm^{-1} corresponding to OH bonds, two narrow and intense bands at 1485 and 950 cm^{-1} are observed that are characteristic of quaternary ammonium cations[1,22,23] and C–N bonds, respectively. Therefore, alkyltrimethylammonium species seem to be intercalated within the structure.

Remarkably, prior to ethanol washing, the two XRD reflections indicating the lamellar mesostructure were missing while narrow and intense XRD peaks of tetramethylammonium chloride (TMACl) were identified (Figure SI-2 in the Supporting Information). This surprising result indicates that the sheets are still exfoliated in the crude synthesis product. It is proposed that TMACl acts as a matrix which prevents mobility and assembly of the single titanate sheets. Ethanol washing removes TMACl and enables postsynthetic stacking of single sheets between dissolved TMA^+ cations, thus acting as intercalated species. This peculiar self-assembly behavior and its dependence upon solvent transfer should be assessed in future work.

Results presented above suggest that tetramethylammonium (NMe_4^+) cations are the interlamellar species, obviously related to the initial Me_3N and Me_2HN complexes. Various lamellar titanates have been reported which are made of Ti–O sheets composed of zigzag ribbons of edge sharing TiO_6 octahedra, with different orderings of these ribbons. $A_2Ti_nO_{2n+1}$ ($n \le 5$), where A^+ is an interlamellar alkali ion or a proton. have been described as corrugated layers with ribbons stepped every nth octahedra,[24] while $Rb_xMn_xTi_{2-x}O_4$,[25] $Cs_2Ti_6O_{13}$,[26] $H_{0.7}Ti_{1.825}O_{4.0}\cdot H_2O$,[19,20] and $NaTi_2O_4(OH)$[21] are reported to be composed of noncorrugated pseudolepidocrocite γ-FeOOH-type layers (Figure SI-3 in the Supporting Information). Though difficult to perform because of fast sample decomposition under the laser beam, Raman investigations (Figure SI-4 in the Supporting Information) provide further insight into the ordering of the Ti–O sheets. While samples obtained with $^tBuH_2N$–BH_3 and pyridine–BH_3 exhibit characteristic bands of anatase at 155 and 205 cm^{-1},[27] titanate samples are strongly different with bands at 155, 210, 285, and 440 cm^{-1}. These data are in agreement with previous results on titanates with a pseudolepidocrocite-type structure.[20] In particular, the absence of a band at 850–950 cm^{-1} indicates that the Ti–O layers do not contain steps and are not corrugated, then suggesting a pseudolepidocrocite-type structure

(22) Hipps, K. W.; Mazur, U. *J. Phys. Chem.* **1987**, *91*, 5218–5224.
(23) Spinner, E. *Spectrochim. Acta Part A: Mol. Biomol. Spectrosc.* **2003**, *59*, 1441–1456.
(24) Kwiatkowska, J.; Grey, I. E.; Madsen, I. C.; Bursill, L. A. *Acta Crystallogr.* **1987**, *B43*, 258–265.
(25) Reid, A. F.; Mumme, W. G.; Wadsley, A. D. *Acta Crystallogr.* **1968**, *B24*, 1228–1233.
(26) Feist, T. P.; Davies, P. K. *J. Solid State Chem.* **1992**, *101*, 275–295.
(27) Ohsaka, T.; Izumi, F.; Fujiki, Y. *J. Raman Spectrosc.* **1978**, *7*, 321–324.

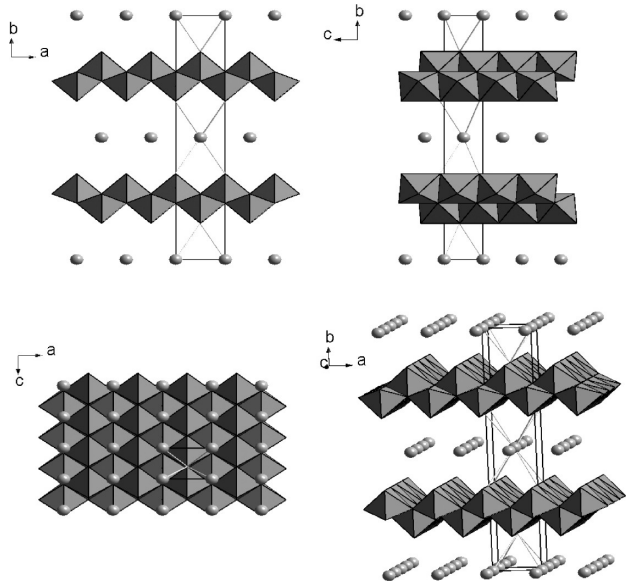

Figure 2. Polyhedral representation of the orthorhombic pseudolepidocrocite-type structural model made of TiO_6 octahedra of the hybrid titanate. Spheres: expected positions of TMA^+ ions.

(Figure SI-3 in the Supporting Information and Figure 2).[21] Cell refinement from the XRD patterns of samples obtained with NPr_3 and NOc_3 was performed, on the basis of the orthorhombic structure of lepidocrocite. The following cell parameters were deduced: $a = 0.375$ nm, $b = 2.311$ nm, $c = 0.295$ nm, where Ti−O layers are stacked perpendicularly to b (Figure 2). In order to evaluate the size of the cavities between the layers, atom positions were derived from lepidocrocite-type $Cs_2Ti_6O_{13}$.[26] The lepidocrocite structure within the (a, c) plane was preserved while the interlamellar distance between the "centers" of two Ti−O sheets was increased to 1.16 nm (Figure 2). Atom coordinates were not refined. From this representation, it is deduced that the cations accommodated between the layers have a diameter of ca. 0.57 nm. Considering the simplicity of the structural model, this value is in good agreement with the TMA^+ ionic diameter of 0.63 nm,[23] thus supporting the hypothesis of TMA^+ ions as the interlamellar species. Therefore the proposed formula for the hybrid titanate is $(N(CH_3)_4)_{0.8}Ti_2O_4(OH)_{0.8(1-x)}O_{0.4\cdot x}$ ($0 \leq x \leq 1$). Even if the amount of hydroxyl and oxo groups within the interlayer[21] as well as the potential presence of titanium vacancies[19,20] could not be accurately evaluated, the hybrid compound presented herein differs strongly from the TMA^+ titanate reported by Liu et al.,[5] which was synthesized in an alkali aqueous medium and exhibited a hexagonal kassite-type structure. The difference between both TMA^+ titanates may come from the nonaqueous route employed in our study, which rules out the eventual presence of water molecules in the interlayer space and causes strong modifications of the condensation pathway for the formation of oxo bridges between Ti(IV) cations.[8] The reaction mechanisms at the molecular scale are investigated further below.

FESEM (Figure 3a) indicates that anatase is composed of nanoparticles of ca. 20 nm in diameter. BET analysis of

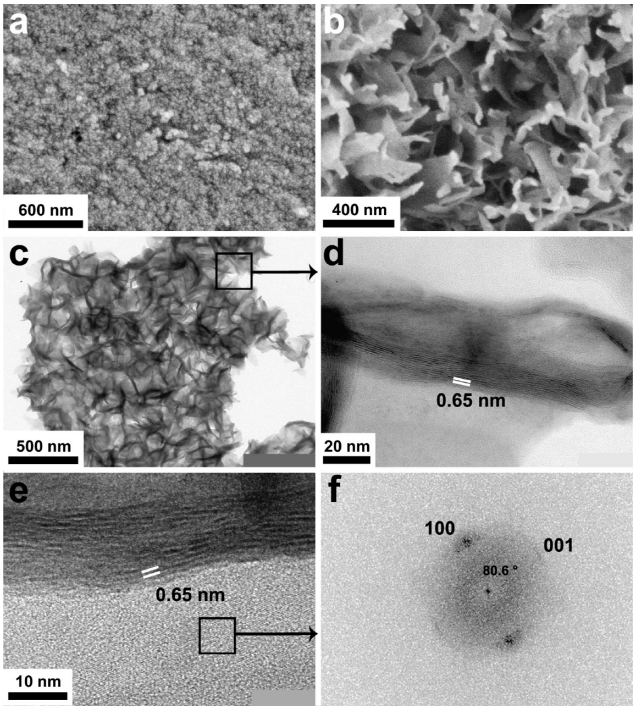

Figure 3. FESEM images of (a) anatase obtained with pyridine−BH_3 and (b) titanate obtained with Me_3N−BH_3 and NPr_3. (c) TEM and (d) HRTEM images of titanate nanosheets obtained with Me_3N−BH_3 and NPr_3. (e) HRTEM image and (f) corresponding FFT analysis of a titanate sheet obtained with Me_3N−BH_3 and NPr_3.

N_2 sorption isotherms shows that anatase samples have a specific surface area (S_{BET}) of ca. 160 $m^2 \cdot g^{-1}$. Titanate samples after washing are composed of sheetlike assemblies (Figures 3b), in good agreement with their primary lamellar structure. TEM (Figure 3c,d) confirms the sheetlike morphology of the titanate with a thickness of ca. 20 nm. Due to fast decomposition of the sample under the electron beam, HRTEM turned out to be difficult to carry out. A lamellar nanostructure was still observed (Figure 3d) with an interlamellar distance of ca. 0.65 nm, lower than the value obtained from XRD because of destruction of the organic moieties during TEM studies. HRTEM investigation of a sheet in the (a, c) plane (Figure 3e,f) shows that disorder as well as a distortion from the orthorhombic structure to a monoclinic one could arise, as recently observed by Peng et al. in pseudolepidocrocite-type $NaTi_2O_4(OH)$.[21] Cell refinement from the XRD patterns by considering this distortion leads to the following parameters: $a = 0.379$ nm, $b = 2.311$ nm, $c = 0.301$ nm, $\beta = 99.6°$. These values are in agreement with HRTEM observations.

Addition of long chain trialkylamines causes strong modifications of the titanate morphology and texture. Indeed, larger basal faces are obtained upon addition of NPr_3 and NOc_3 when compared to solely Me_3N−BH_3 (Figure 4). Thus, preferential growth of the single sheets seems to be facilitated by the long chain trialkylamines which could act as effective stabilizers for the surface. These results suggest that preferential complexation of the amines occurs on the basal (010) faces. The bulky amphiphilic amines are nevertheless not assembled

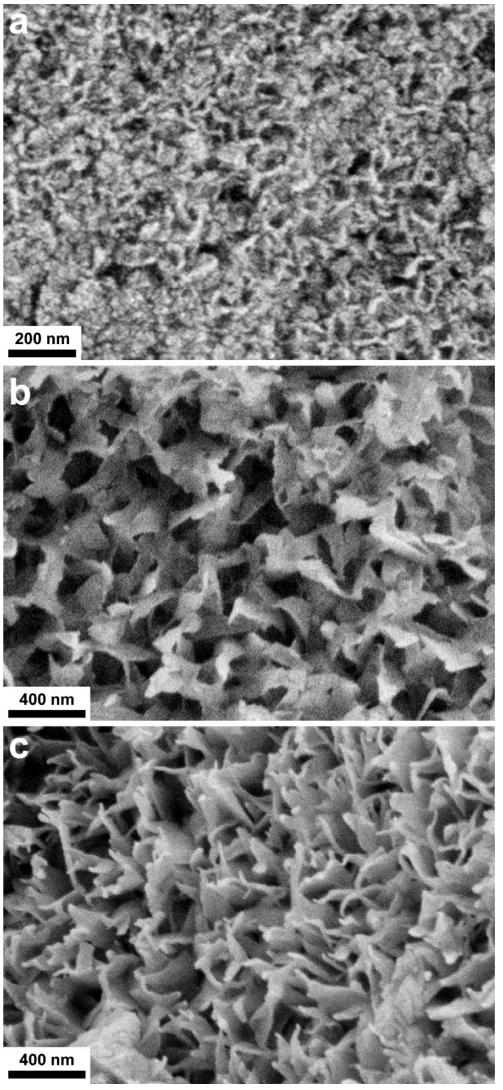

Figure 4. FESEM images of samples obtained with (a) Me_3N-BH_3, (b) Me_3N-BH_3 and NPr_3, and (c) Me_3N-BH_3 and NOc_3.

between the layers during the final aggregation process. When Me_3N-BH_3 is solely used, small amounts of a byproduct, isotropic anatase nanoparticles of ca. 5 nm in diameter, are identified by TEM (Figure SI-5 in the Supporting Information). Pure titanates obtained with NPr_3 and NOc_3 exhibit a specific surface area S_{BET} of 100 $m^2 \cdot g^{-1}$, while desorption isotherms (Figure SI-6 in the Supporting Information) reveal a strong drop of adsorbed volume at $P/P^\circ \approx 0.47$, indicating an "ink-bottle" effect of a pore system accessed over small entries. For samples obtained with Me_3N-BH_3 as single reagent, the S_{BET} is 220 $m^2 \cdot g^{-1}$. This high value compared to pure titanate is attributed to much smaller titanate nanosheets and, to a minor extent, to the anatase byproduct.

It is rather surprising that oxides form in the absence of any initial water or alcohol. Actually, the polyether solvent triglyme is the only potential oxygen donor. To understand the reaction pathways leading to the Ti−O network and to TMA^+ intercalated ions, gas chromatography coupled mass spectrometry (GC-MS) was performed on the resulting supernatants. Alkylchlorides and ethers derived from triglyme were observed (Scheme 1)

Scheme 1. Reactions Involved in the Formation of Alkylchlorides and Ethers[a]

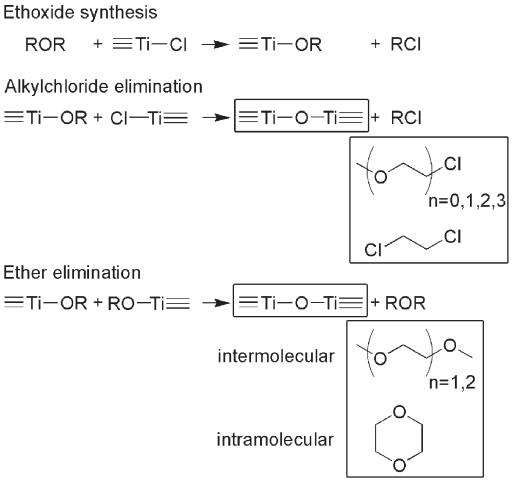

[a] Enclosed molecular structures correspond to species identified by XRD of the solid before washing and GC-MS of the supernatant.

Scheme 2. Reactions Involved in the Formation of Nitrogen Containing Species[a]

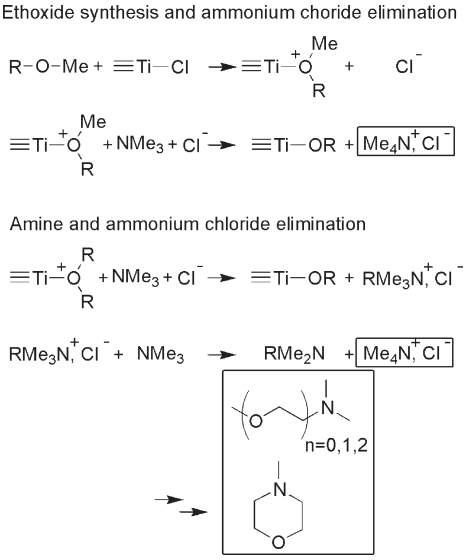

[a] Enclosed molecular structures correspond to species identified by XRD of the solid before washing and GC-MS of the supernatant.

and are explained by classical reactions of nonaqueous nanoparticle syntheses, such as titanium ethoxide formation and alkylchloride and ether elimination.[8,9] These species have also been observed in a blank synthesis where only $TiCl_4$ was dissolved in triglyme. Nevertheless, this procedure led to pure anatase, without any mesostructure. In addition to chlorides and ethers, nitrogen derivatives of triglyme and trimethylamine (NMe_3) were observed (Scheme 2). It is proposed that triglyme could be activated by Ti(IV) complexation, thus undergoing NMe_3 nucleophilic attack and leading to a titanium ethoxide bond and tetramethylammonium. In parallel, boron is observed as being involved in the dioxaborolane **1** with a B−C bond (Scheme 3). The dioxaborolane cycle can be explained by alkane elimination from the Ti(IV) activated triglyme, as observed during the deprotection of

Scheme 3. Reactions Involving Boron Species[a]

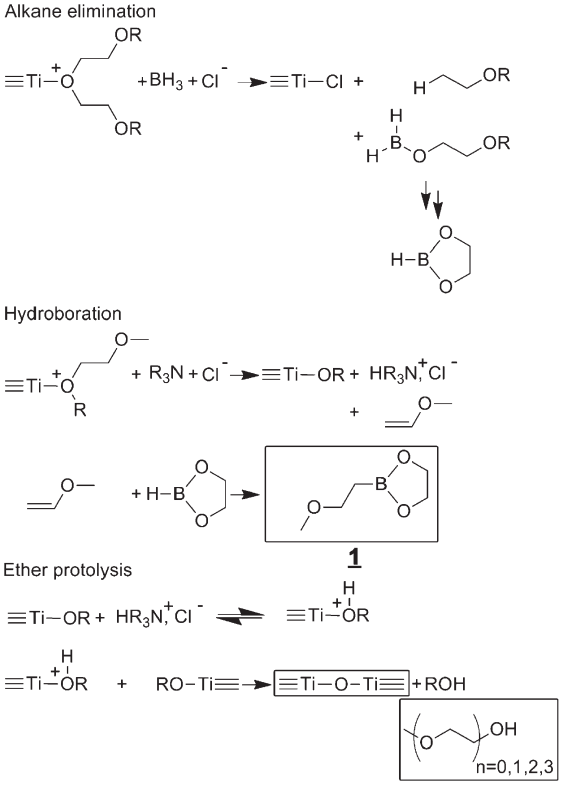

[a] Enclosed molecular structures correspond to species identified by XRD of the solid before washing and GC-MS of the supernatant.

acetals with BH_3 adducts in the presence of a Lewis acid.[28] The B−C bond originates from hydroboration on a C=C double bond. Indeed, an alkene can be formed by elimination through the action of the trialkylamine as a base on the activated triglyme, leading to a titanium ethoxide bond, a trialkylammonium ion, and an alkene. The latter can, therefore, undergo hydroboration, leading to **1**. Interestingly, alcohols derived from triglyme were also observed. Due to the polarity of the B−H bond, borane BH_3 cannot account for the formation of alcohols which implies protons. It is, therefore, proposed that the protonated amine obtained during the alkene formation reacts with titanium ethoxide, which then undergoes condensation and alcohol elimination. No hybrid titanate was observed in the case of $^tBuH_2N{-}BH_3$ and pyridine$-BH_3$ precursors since no TMA^+ ions could be formed. Noteworthy, from the mechanism described above, BH_3 should not be essential to the formation of TMA^+ ions. Indeed, a synthesis performed by mixing NEt_3 and $TiCl_4$ in triglyme led also to the hybrid titanate. However, upon addition of NEt_3 to $TiCl_4$, an insoluble adduct[29] was formed and a heterogeneous morphology for the final sample was obtained. On the contrary, $Me_3N{-}BH_3$ prevents complexation of Ti(IV) by the amine. Since BH_3 acts as an amine sequester through strong complexation, a clear homogeneous initial solution is formed. Thus, the

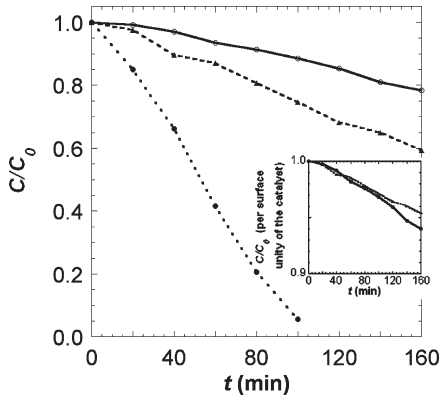

Figure 5. Photocalytic decomposition of 4-chlorophenol under a Xe lamp (irradiation wavelength > 300 nm) in the presence of pure titanate obtained with $Me_3N{-}BH_3$ and NPr_3 (solid line), titanate/anatase mixture obtained with $Me_3N{-}BH_3$ (dashed line), and commercial Degussa P25 (dotted line). Inset: 4-chlorophenol decomposition normalized versus the surface area of pure titanate (90 $m^2 \cdot g^{-1}$) and titanate/anatase mixture (220 $m^2 \cdot g^{-1}$).

primary role of BH_3 is to provide a stable amine complex that is less reactive toward Ti(IV) and leads to an homogeneous product, with good control of the nanoscaled morphology.

A preliminary evaluation of the photocatalytic activity was carried out by following the decomposition of 4-chlorophenol in water under a Xe lamp and in the presence of a known amount of sample (see Supporting Information). A titanate/anatase mixture obtained with $Me_3N{-}BH_3$, a pure titanate sample obtained by addition of NPr_3, and Degussa P25 as a reference were investigated (Figure 5 and Figure SI-7 in the Supporting Information). The experimentally determined activities are lower than commercial P25 but similar to those reported for different titanates by other groups.[2] The rate of degradation is higher for the high surface area sample. Normalizing the curves by the surface area for each sample shows that the specific surface activities are close to each other (Figure 5 inset); i.e., the influence of the anatase byproduct can be neglected. Significantly, the slope for the decomposition curve of pure titanate is becoming more negative with illumination time. The XRD pattern of the catalyst separated from the solution after UV exposition indicates that titanate was partially converted into anatase and rutile TiO_2. The organic−inorganic hybrid nanostructure is presumably not photostable against the self-generated $^{\bullet}OH$ radicals during the photocatalysis process. However, the increase of activity shows that the hybrid titanate behaves as a precursor for in situ formation of an efficient TiO_2 based photocatalyst.

Conclusion

In summary, a novel hybrid titanate with lamellar nanostructures has been obtained by a nonaqueous route. Reaction pathways were elucidated, where the polyether solvent at 220 °C acts as oxygen donor for the Ti−O framework, while an amine−borane reagent leads to the in situ formation of tetramethylammonium cations intercalated into the lamellar structure. Structural control was

(28) Johnsson, R.; Olsson, D.; Ellervik, U. *J. Org. Chem.* **2008**, *73*, 5226–5232.
(29) Feld, R.; Cowe, P. L. *The Organic Chemistry of Titanium*; Butterworths: Washington, D.C., 1965.

demonstrated by modifying the nature of the amine precursor, while the morphology of the titanate nanosheets could be tuned by addition of long chain trialkylamines acting as a surface stabilizer. Photocatalytic activity of the nanostructured titanate could be proven, which depends on the resulting texture of these compounds. This study demonstrates the high potential of nonaqueous routes for the design of functional nanostructured titanates. From a more fundamental point of view, this work also highlights self-assembly as a milestone for the formation of new titanate nanostructures. This key issue will be addressed in future works.

Acknowledgment. The authors acknowledge the Max-Planck-Institute-CNRS Postdoctoral Program for Nanomaterials for financial support, Ms. Xiufang Chen (MPIKG) and Dr. XinChen Wang (MPIKG) for their help on photocatalysis experiments, Rona Pitschke (MPIKG) for FESEM, Dr. Patricia Beaunier (UPMC) for HRTEM, and Dr. Hendrik Wetzel (Fraunhofer Institute für Angewandte Polymerforschung) for elemental analysis.

Supporting Information Available: Infrared spectra of titanate samples, XRD patterns before and after ethanol washing, representation of the lepidocrocite structure, Raman spectra of pure anatase and of an anatase−titanate composite, (HR)TEM images of anatase nanoparticles within the sample obtained with solely Me_3N-BH_3, N_2 sorption isotherm of a titanate sample (PDF). This material is available free of charge via the Internet at http://pubs.acs.org.